2014-11

Measurements of Direct CP Asymmetries in $B \to X_s \gamma$ Decays using Sum of Exclusive Decays

UTD AUTHOR(S): Joseph M. Izen and Xinchou Lou

Lees, J. P., V. Poireau, V. Tisserand, E. Grauges, et al. 2014. "Measurements of direct CP asymmetries in $B \to X_s \gamma$ decays using sum of exclusive decays." Physical Review D 90(9): 092001.

Measurements of direct *CP* asymmetries in $B \to X_s\gamma$ decays using sum of exclusive decays

J. P. Lees,[1] V. Poireau,[1] V. Tisserand,[1] E. Grauges,[2] A. Palano,[3a,3b] G. Eigen,[4] B. Stugu,[4] D. N. Brown,[5] L. T. Kerth,[5] Yu. G. Kolomensky,[5] M. J. Lee,[5] G. Lynch,[5] H. Koch,[6] T. Schroeder,[6] C. Hearty,[7] T. S. Mattison,[7] J. A. McKenna,[7] R. Y. So,[7] A. Khan,[8] V. E. Blinov,[9a,9c] A. R. Buzykaev,[9a] V. P. Druzhinin,[9a,9b] V. B. Golubev,[9a,9b] E. A. Kravchenko,[9a,9b] A. P. Onuchin,[9a,9c] S. I. Serednyakov,[9a,9b] Yu. I. Skovpen,[9a,9b] E. P. Solodov,[9a,9b] K. Yu. Todyshev,[9a,9b] A. N. Yushkov,[9a] D. Kirkby,[10] A. J. Lankford,[10] M. Mandelkern,[10] B. Dey,[11] J. W. Gary,[11] O. Long,[11] C. Campagnari,[12] M. Franco Sevilla,[12] T. M. Hong,[12] D. Kovalskyi,[12] J. D. Richman,[12] C. A. West,[12] A. M. Eisner,[13] W. S. Lockman,[13] B. A. Schumm,[13] A. Seiden,[13] D. S. Chao,[14] C. H. Cheng,[14] B. Echenard,[14] K. T. Flood,[14] D. G. Hitlin,[14] P. Ongmongkolkul,[14] F. C. Porter,[14] R. Andreassen,[15] Z. Huard,[15] B. T. Meadows,[15] B. G. Pushpawela,[15] M. D. Sokoloff,[15] L. Sun,[15] P. C. Bloom,[16] W. T. Ford,[16] A. Gaz,[16] U. Nauenberg,[16] J. G. Smith,[16] S. R. Wagner,[16] R. Ayad,[17,†] W. H. Toki,[17] B. Spaan,[18] R. Schwierz,[19] D. Bernard,[20] M. Verderi,[20] S. Playfer,[21] D. Bettoni,[22a] C. Bozzi,[22a] R. Calabrese,[22a,22b] G. Cibinetto,[22a,22b] E. Fioravanti,[22a,22b] I. Garzia,[22a,22b] E. Luppi,[22a,22b] L. Piemontese,[22a] V. Santoro,[22a] R. Baldini-Ferroli,[23] A. Calcaterra,[23] R. de Sangro,[23] G. Finocchiaro,[23] S. Martellotti,[23] P. Patteri,[23] I. M. Peruzzi,[23,‡] M. Piccolo,[23] M. Rama,[23] A. Zallo,[23] R. Contri,[24a,24b] E. Guido,[24a,24b] M. Lo Vetere,[24a,24b] M. R. Monge,[24a,24b] S. Passaggio,[24a] C. Patrignani,[24a,24b] E. Robutti,[24a] B. Bhuyan,[25] V. Prasad,[25] M. Morii,[26] A. Adametz,[27] U. Uwer,[27] H. M. Lacker,[28] P. D. Dauncey,[29] U. Mallik,[30] C. Chen,[31] J. Cochran,[31] W. T. Meyer,[31] S. Prell,[31] H. Ahmed,[32] A. V. Gritsan,[33] N. Arnaud,[34] M. Davier,[34] D. Derkach,[34] G. Grosdidier,[34] F. Le Diberder,[34] A. M. Lutz,[34] B. Malaescu,[34,§] P. Roudeau,[34] A. Stocchi,[34] G. Wormser,[34] D. J. Lange,[35] D. M. Wright,[35] J. P. Coleman,[36] J. R. Fry,[36] E. Gabathuler,[36] D. E. Hutchcroft,[36] D. J. Payne,[36] C. Touramanis,[36] A. J. Bevan,[37] F. Di Lodovico,[37] R. Sacco,[37] G. Cowan,[38] J. Bougher,[39] D. N. Brown,[39] C. L. Davis,[39] A. G. Denig,[40] M. Fritsch,[40] W. Gradl,[40] K. Griessinger,[40] A. Hafner,[40] E. Prencipe,[40] K. R. Schubert,[40] R. J. Barlow,[41,¶] G. D. Lafferty,[41] E. Behn,[42] R. Cenci,[42] B. Hamilton,[42] A. Jawahery,[42] D. A. Roberts,[42] R. Cowan,[43] D. Dujmic,[43] G. Sciolla,[43] R. Cheaib,[44] P. M. Patel,[44,*] S. H. Robertson,[44] P. Biassoni,[45a,45b] N. Neri,[45a] F. Palombo,[45a,45b] L. Cremaldi,[46] R. Godang,[46,**] P. Sonnek,[46] D. J. Summers,[46] M. Simard,[47] P. Taras,[47] G. De Nardo,[48a,48b] D. Monorchio,[48a,48b] G. Onorato,[48a,48b] C. Sciacca,[48a,48b] M. Martinelli,[49] G. Raven,[49] C. P. Jessop,[50] J. M. LoSecco,[50] K. Honscheid,[51] R. Kass,[51] J. Brau,[52] R. Frey,[52] N. B. Sinev,[52] D. Strom,[52] E. Torrence,[52] H. Ahmed,[32] E. Feltresi,[53a,53b] M. Margoni,[53a,53b] M. Morandin,[53a] M. Posocco,[53a] M. Rotondo,[53a] G. Simi,[53a] F. Simonetto,[53a,53b] R. Stroili,[53a,53b] S. Akar,[54] E. Ben-Haim,[54] M. Bomben,[54] G. R. Bonneaud,[54] H. Briand,[54] G. Calderini,[54] J. Chauveau,[54] Ph. Leruste,[54] G. Marchiori,[54] J. Ocariz,[54] S. Sitt,[54] M. Biasini,[55a,55b] E. Manoni,[55a] S. Pacetti,[55a,55b] A. Rossi,[55a] C. Angelini,[56a,56b] G. Batignani,[56a,56b] S. Bettarini,[56a,56b] M. Carpinelli,[56a,56b,††] G. Casarosa,[56a,56b] A. Cervelli,[56a,56b] F. Forti,[56a,56b] M. A. Giorgi,[56a,56b] A. Lusiani,[56a,56c] B. Oberhof,[56a,56b] E. Paoloni,[56a,56b] A. Perez,[56a] G. Rizzo,[56a,56b] J. J. Walsh,[56a] D. Lopes Pegna,[57] J. Olsen,[57] A. J. S. Smith,[57] R. Faccini,[58a,58b] F. Ferrarotto,[58a] F. Ferroni,[58a,58b] M. Gaspero,[58a,58b] L. Li Gioi,[58a] G. Piredda,[58a] C. Bünger,[59] O. Grünberg,[59] T. Hartmann,[59] T. Leddig,[59] C. Voß,[59] R. Waldi,[59] T. Adye,[60] E. O. Olaiya,[60] F. F. Wilson,[60] S. Emery,[61] G. Hamel de Monchenault,[61] G. Vasseur,[61] Ch. Yèche,[61] F. Anulli,[62,‡‡] D. Aston,[62] D. J. Bard,[62] J. F. Benitez,[62] C. Cartaro,[62] M. R. Convery,[62] J. Dorfan,[62] G. P. Dubois-Felsmann,[62] W. Dunwoodie,[62] M. Ebert,[62] R. C. Field,[62] B. G. Fulsom,[62] A. M. Gabareen,[62] M. T. Graham,[62] C. Hast,[62] W. R. Innes,[62] P. Kim,[62] M. L. Kocian,[62] D. W. G. S. Leith,[62] P. Lewis,[62] D. Lindemann,[62] B. Lindquist,[62] S. Luitz,[62] V. Luth,[62] H. L. Lynch,[62] D. B. MacFarlane,[62] D. R. Muller,[62] H. Neal,[62] S. Nelson,[62] M. Perl,[62] T. Pulliam,[62] B. N. Ratcliff,[62] A. Roodman,[62] A. A. Salnikov,[62] R. H. Schindler,[62] A. Snyder,[62] D. Su,[62] M. K. Sullivan,[62] J. Va'vra,[62] A. P. Wagner,[62] W. F. Wang,[62] W. J. Wisniewski,[62] M. Wittgen,[62] D. H. Wright,[62] H. W. Wulsin,[62] V. Ziegler,[62] W. Park,[63] M. V. Purohit,[63] R. M. White,[63,§§] J. R. Wilson,[63] A. Randle-Conde,[64] S. J. Sekula,[64] M. Bellis,[65] P. R. Burchat,[65] T. S. Miyashita,[65] E. M. T. Puccio,[65] M. S. Alam,[66] J. A. Ernst,[66] R. Gorodeisky,[67] N. Guttman,[67] D. R. Peimer,[67] A. Soffer,[67] S. M. Spanier,[68] J. L. Ritchie,[69] A. M. Ruland,[69] R. F. Schwitters,[69] B. C. Wray,[69] J. M. Izen,[70] X. C. Lou,[70] F. Bianchi,[71a,71b] F. De Mori,[71a,71b] A. Filippi,[71a] D. Gamba,[71a,71b] S. Zambito,[71a,71b] L. Lanceri,[72a,72b] L. Vitale,[72a,72b] F. Martinez-Vidal,[73] A. Oyanguren,[73] P. Villanueva-Perez,[73] J. Albert,[74] Sw. Banerjee,[74] F. U. Bernlochner,[74] H. H. F. Choi,[74] G. J. King,[74] R. Kowalewski,[74] M. J. Lewczuk,[74] T. Lueck,[74] I. M. Nugent,[74] J. M. Roney,[74] R. J. Sobie,[74] N. Tasneem,[74] T. J. Gershon,[75] P. F. Harrison,[75] T. E. Latham,[75] H. R. Band,[76] S. Dasu,[76] Y. Pan,[76] R. Prepost,[76] and S. L. Wu[76]

(*BABAR* Collaboration)

[1]*Laboratoire d'Annecy-le-Vieux de Physique des Particules (LAPP), Université de Savoie, CNRS/IN2P3, F-74941 Annecy-Le-Vieux, France*
[2]*Universitat de Barcelona, Facultat de Fisica, Departament ECM, E-08028 Barcelona, Spain*
[3a]*INFN Sezione di Bari, I-70126 Bari, Italy*
[3b]*Dipartimento di Fisica, Università di Bari, I-70126 Bari, Italy*

[4]*University of Bergen, Institute of Physics, N-5007 Bergen, Norway*
[5]*Lawrence Berkeley National Laboratory and University of California, Berkeley, California 94720, USA*
[6]*Ruhr Universität Bochum, Institut für Experimentalphysik 1, D-44780 Bochum, Germany*
[7]*University of British Columbia, Vancouver, British Columbia, Canada V6T 1Z1*
[8]*Brunel University, Uxbridge, Middlesex UB8 3PH, United Kingdom*
[9a]*Budker Institute of Nuclear Physics SB RAS, Novosibirsk 630090, Russia*
[9b]*Novosibirsk State University, Novosibirsk 630090, Russia*
[9c]*Novosibirsk State Technical University, Novosibirsk 630092, Russia*
[10]*University of California at Irvine, Irvine, California 92697, USA*
[11]*University of California at Riverside, Riverside, California 92521, USA*
[12]*University of California at Santa Barbara, Santa Barbara, California 93106, USA*
[13]*University of California at Santa Cruz, Institute for Particle Physics, Santa Cruz, California 95064, USA*
[14]*California Institute of Technology, Pasadena, California 91125, USA*
[15]*University of Cincinnati, Cincinnati, Ohio 45221, USA*
[16]*University of Colorado, Boulder, Colorado 80309, USA*
[17]*Colorado State University, Fort Collins, Colorado 80523, USA*
[18]*Technische Universität Dortmund, Fakultät Physik, D-44221 Dortmund, Germany*
[19]*Technische Universität Dresden, Institut für Kern- und Teilchenphysik, D-01062 Dresden, Germany*
[20]*Laboratoire Leprince-Ringuet, Ecole Polytechnique, CNRS/IN2P3, F-91128 Palaiseau, France*
[21]*University of Edinburgh, Edinburgh EH9 3JZ, United Kingdom*
[22a]*INFN Sezione di Ferrara, I-44122 Ferrara, Italy*
[22b]*Dipartimento di Fisica e Scienze della Terra, Università di Ferrara, I-44122 Ferrara, Italy*
[23]*INFN Laboratori Nazionali di Frascati, I-00044 Frascati, Italy*
[24a]*INFN Sezione di Genova, I-16146 Genova, Italy*
[24b]*Dipartimento di Fisica, Università di Genova, I-16146 Genova, Italy*
[25]*Indian Institute of Technology Guwahati, Guwahati, Assam, 781 039, India*
[26]*Harvard University, Cambridge, Massachusetts 02138, USA*
[27]*Universität Heidelberg, Physikalisches Institut, D-69120 Heidelberg, Germany*
[28]*Humboldt-Universität zu Berlin, Institut für Physik, D-12489 Berlin, Germany*
[29]*Imperial College London, London, SW7 2AZ, United Kingdom*
[30]*University of Iowa, Iowa City, Iowa 52242, USA*
[31]*Iowa State University, Ames, Iowa 50011-3160, USA*
[32]*Jazan University, Jazan 22822, Kingdom of Saudi Arabia*
[33]*Johns Hopkins University, Baltimore, Maryland 21218, USA*
[34]*Laboratoire de l'Accélérateur Linéaire, IN2P3/CNRS et Université Paris-Sud 11, Centre Scientifique d'Orsay, F-91898 Orsay Cedex, France*
[35]*Lawrence Livermore National Laboratory, Livermore, California 94550, USA*
[36]*University of Liverpool, Liverpool L69 7ZE, United Kingdom*
[37]*Queen Mary, University of London, London, E1 4NS, United Kingdom*
[38]*University of London, Royal Holloway and Bedford New College, Egham, Surrey TW20 0EX, United Kingdom*
[39]*University of Louisville, Louisville, Kentucky 40292, USA*
[40]*Johannes Gutenberg-Universität Mainz, Institut für Kernphysik, D-55099 Mainz, Germany*
[41]*University of Manchester, Manchester M13 9PL, United Kingdom*
[42]*University of Maryland, College Park, Maryland 20742, USA*
[43]*Massachusetts Institute of Technology, Laboratory for Nuclear Science, Cambridge, Massachusetts 02139, USA*
[44]*McGill University, Montréal, Québec, Canada H3A 2T8*
[45a]*INFN Sezione di Milano, I-20133 Milano, Italy*
[45b]*Dipartimento di Fisica, Università di Milano, I-20133 Milano, Italy*
[46]*University of Mississippi, University, Mississippi 38677, USA*
[47]*Université de Montréal, Physique des Particules, Montréal, Québec, Canada H3C 3J7*
[48a]*INFN Sezione di Napoli, I-80126 Napoli, Italy*
[48b]*Dipartimento di Scienze Fisiche, Università di Napoli Federico II, I-80126 Napoli, Italy*
[49]*NIKHEF, National Institute for Nuclear Physics and High Energy Physics, NL-1009 DB Amsterdam, The Netherlands*
[50]*University of Notre Dame, Notre Dame, Indiana 46556, USA*
[51]*Ohio State University, Columbus, Ohio 43210, USA*
[52]*University of Oregon, Eugene, Oregon 97403, USA*
[53a]*INFN Sezione di Padova, I-35131 Padova, Italy*

[53b]*Dipartimento di Fisica, Università di Padova, I-35131 Padova, Italy*
[54]*Laboratoire de Physique Nucléaire et de Hautes Energies, IN2P3/CNRS, Université Pierre et Marie Curie-Paris6, Université Denis Diderot-Paris7, F-75252 Paris, France*
[55a]*INFN Sezione di Perugia, I-06123 Perugia, Italy*
[55b]*Dipartimento di Fisica, Università di Perugia, I-06123 Perugia, Italy*
[56a]*INFN Sezione di Pisa, I-56127 Pisa, Italy*
[56b]*Dipartimento di Fisica, Università di Pisa, I-56127 Pisa, Italy*
[56c]*Scuola Normale Superiore di Pisa, I-56127 Pisa, Italy*
[57]*Princeton University, Princeton, New Jersey 08544, USA*
[58a]*INFN Sezione di Roma, I-00185 Roma, Italy*
[58b]*Dipartimento di Fisica, Università di Roma La Sapienza, I-00185 Roma, Italy*
[59]*Universität Rostock, D-18051 Rostock, Germany*
[60]*Rutherford Appleton Laboratory, Chilton, Didcot, Oxon OX11 0QX, United Kingdom*
[61]*CEA, Irfu, SPP, Centre de Saclay, F-91191 Gif-sur-Yvette, France*
[62]*SLAC National Accelerator Laboratory, Stanford, California 94309, USA*
[63]*University of South Carolina, Columbia, South Carolina 29208, USA*
[64]*Southern Methodist University, Dallas, Texas 75275, USA*
[65]*Stanford University, Stanford, California 94305-4060, USA*
[66]*State University of New York, Albany, New York 12222, USA*
[67]*Tel Aviv University, School of Physics and Astronomy, Tel Aviv, 69978, Israel*
[68]*University of Tennessee, Knoxville, Tennessee 37996, USA*
[69]*University of Texas at Austin, Austin, Texas 78712, USA*
[70]*University of Texas at Dallas, Richardson, Texas 75083, USA*
[71a]*INFN Sezione di Torino, I-10125 Torino, Italy*
[71b]*Dipartimento di Fisica, Università di Torino, I-10125 Torino, Italy*
[72a]*INFN Sezione di Trieste, I-34127 Trieste, Italy*
[72b]*Dipartimento di Fisica, Università di Trieste, I-34127 Trieste, Italy*
[73]*IFIC, Universitat de Valencia-CSIC, E-46071 Valencia, Spain*
[74]*University of Victoria, Victoria, British Columbia, Canada V8W 3P6*
[75]*Department of Physics, University of Warwick, Coventry CV4 7AL, United Kingdom*
[76]*University of Wisconsin, Madison, Wisconsin 53706, USA*
(Received 4 June 2014; published 5 November 2014)

We measure the direct *CP* violation asymmetry, A_{CP}, in $B \to X_s\gamma$ and the isospin difference of the asymmetry, ΔA_{CP}, using 429 fb^{-1} of data collected at $\Upsilon(4S)$ resonance with the *BABAR* detector at the PEP-II asymmetric-energy e^+e^- storage rings operating at the SLAC National Accelerator Laboratory. B mesons are reconstructed from ten charged B final states and six neutral B final states. We find $A_{CP} = +(1.7 \pm 1.9 \pm 1.0)\%$, which is in agreement with the Standard Model prediction and provides an improvement on the world average. Moreover, we report the first measurement of the difference between A_{CP} for charged and neutral decay modes, $\Delta A_{CP} = +(5.0 \pm 3.9 \pm 1.5)\%$. Using the value of ΔA_{CP}, we also provide 68% and 90% confidence intervals on the imaginary part of the ratio of the Wilson coefficients corresponding to the chromomagnetic dipole and the electromagnetic dipole transitions.

DOI: 10.1103/PhysRevD.90.092001 PACS numbers: 13.20.-v, 13.25.Hw

I. INTRODUCTION

The flavor-changing neutral current decay $B \to X_s\gamma$, where X_s represents any hadronic system with one unit of strangeness, is highly suppressed in the standard model (SM), as is the direct *CP* asymmetry,

$$A_{CP} = \frac{\Gamma_{\bar{B}^0/B^- \to X_s\gamma} - \Gamma_{B^0/B^+ \to X_{\bar{s}}\gamma}}{\Gamma_{\bar{B}^0/B^- \to X_s\gamma} + \Gamma_{B^0/B^+ \to X_{\bar{s}}\gamma}}, \tag{1}$$

due to the combination of CKM and GIM suppressions [1]. New physics effects could enhance the asymmetry to a level as large as 15% [2–4]. The current world average of

[*]Deceased.
[†]Now at the University of Tabuk, Tabuk 71491, Saudi Arabia.
[‡]Also with Università di Perugia, Dipartimento di Fisica, Perugia, Italy.
[§]Now at Laboratoire de Physique Nucláire et de Hautes Energies, IN2P3/CNRS, Paris, France.
[‖]Now at the University of Huddersfield, Huddersfield HD1 3DH, United Kingdom.
[¶]Now at University of South Alabama, Mobile, Alabama 36688, USA.
[**]Also with Università di Sassari, Sassari, Italy.
[††]Also with INFN Sezione di Roma, Roma, Italy.
[‡‡]Now at Universidad Técnica Federico Santa Maria, Valparaiso, Chile 2390123.

A_{CP} based on the results from *BABAR* [5], Belle [6] and CLEO [7] is $-(0.8 \pm 2.9)\%$ [8]. The SM prediction for the asymmetry was found in a recent study to be long distance dominated [9] and to be in the range $-0.6\% < A_{CP}^{\rm SM} < 2.8\%$.

Benzke *et al.* [9] predict a difference in direct *CP* asymmetry for charged and neutral B mesons,

$$\Delta A_{X_s\gamma} = A_{B^\pm \to X_s\gamma} - A_{B^0/\bar{B}^0 \to X_s\gamma}, \tag{2}$$

which suggests a new test of the SM. The difference, $\Delta A_{X_s\gamma}$, arises from an interference term in A_{CP} that depends on the charge of the spectator quark. The magnitude of $\Delta A_{X_s\gamma}$ is proportional to $\mathrm{Im}(C_{8g}/C_{7\gamma})$ where $C_{7\gamma}$ and C_{8g} are Wilson coefficients corresponding to the electromagnetic dipole and the chromomagnetic dipole transitions, respectively. The two coefficients are real in the SM; therefore, $\Delta A_{X_s\gamma} = 0$. New physics contributions from the enhancement of the *CP*-violating phase or of the magnitude of the two Wilson coefficients [1,10], or the introduction of new operators [11], could enhance $\Delta A_{X_s\gamma}$ to be as large as 10% [9]. Unlike $C_{7\gamma}$, C_{8g} currently does not have a strong experimental constraint [12]. Thus a measurement of $\Delta A_{X_s\gamma}$ together with the existing constraints on $C_{7\gamma}$ can provide a constraint on C_{8g}.

Experimental studies of $B \to X_s\gamma$ are approached in one of two ways. The inclusive approach relies entirely on observation of the high-energy photon from these decays without reconstruction of the hadronic system X_s. By ignoring the X_s system, this approach is sensitive to the full $b \to s\gamma$ decay rate and is robust against final state fragmentation effects. The semi-inclusive approach reconstructs the X_s system in as many specific final state configurations as practical. This approach provides additional information, but since not all X_s final states can be reconstructed without excessive background, fragmentation model-dependence is introduced if semi-inclusive measurements are extrapolated to the complete ensemble of $B \to X_s\gamma$ decays. *BABAR* has recently published results on the $B \to X_s\gamma$ branching fraction and photon spectrum for both approaches [13,14]. The inclusive approach has also been used to search for direct *CP* violation, but since the inclusive method does not distinguish hadronic final states, decays due to $b \to d\gamma$ transitions are included.

We report herein a measurement of A_{CP} and the first measurement of $\Delta A_{X_s\gamma}$ using the semi-inclusive approach with the full *BABAR* data set. We reconstruct 38 exclusive B -decay modes, listed in Table I, but for use in this analysis a subset of 16 modes (marked with an asterisk in Table I) is chosen for which high statistical significance is achieved. Also, for this analysis, modes must be flavor self-tagging (i.e., the bottomness can be determined from the reconstructed final state). The 16 modes include ten charged B and six neutral B decays. After all event selection criteria are applied, the mass of the hadronic X_s system (m_{X_s}) in this measurement covers the range of about 0.6 to 2.0 GeV/c^2. The upper edge of this range approximately corresponds to a minimum photon energy in the B rest frame of 2.3 GeV. For $B \to X_s\gamma$ decays with $0.6 < m_{X_s} < 2.0$ GeV/c^2, the ten charged B modes used account for about 52% of all $B^+ \to X_s\gamma$ decays and the six neutral modes account for about 34% of all neutral $B^0 \to X_s\gamma$ decays.[1] In this analysis it is assumed that A_{CP} and $\Delta A_{X_s\gamma}$ are independent of final state fragmentation. That is, it is assumed that A_{CP} and $\Delta A_{X_s\gamma}$ are independent of the specific X_s final states used for this analysis and independent of the m_{X_s} distribution of the selected events.

II. ANALYSIS OVERVIEW

With data from the *BABAR* detector (Sec. III), we reconstructed B candidates from various final states (Sec. IV). We then trained two multivariate classifiers (Sec. V): one to separate correctly reconstructed B decays from misreconstructed events and the other to reject the continuum background, $e^+e^- \to q\bar{q}$, where $q = u, d, s, c$. The output of the first classifier is used to select the best B candidate for each event. Then, the outputs from both classifiers are used to reject backgrounds. We use the remaining events to determine the asymmetries.

We use identical procedures to extract three asymmetries: the asymmetries of charged and neutral B mesons, and of the combined sample, and the difference, $\Delta A_{X_s\gamma}$. The bottomness of the B meson is determined by the charge of the kaon for B^0 and $\bar{B}^0$, and by the total charge of the reconstructed B meson for B^+ and B^-.

We can decompose A_{CP} into three components:

$$A_{CP} = A_{\rm peak} - A_{\rm det} + D, \tag{3}$$

where $A_{\rm peak}$ is the fitted asymmetry of the events in the peak of the $m_{\rm ES}$ distribution (Sec. VI), $A_{\rm det}$ is the detector asymmetry due to the difference in K^+ and K^- efficiency (Sec. VII), and D is the bias due to peaking background contamination (Sec. VIII). In this analysis we establish upper bounds on the magnitude of D, and then treat those as systematic errors.

III. DETECTOR AND DATA

We use a data sample of 429 fb^{-1} [15] collected at the $\Upsilon(4S)$ resonance, $\sqrt{s} = 10.58$ GeV/c^2, with the *BABAR* detector at the PEP-II asymmetric-energy B factory at the SLAC National Accelerator Laboratory. The data correspond to 471×10^6 produced $B\bar{B}$ pairs.

The *BABAR* detector and its operation are described in detail elsewhere [16,17]. The charges and momenta of charged particles are measured by a five-layer double-sided

[1]If we include K_L modes as if they have same branching fraction as K_S modes, the final state coverage for $0.6 < m_{X_s} < 2.0$ GeV/c^2 is 69% for charged B and 34% for neutral B.

silicon strip detector (SVT) and a 40-layer drift chamber (DCH) operated in a 1.5 T solenoidal field. Charged K/π separation is achieved using dE/dx information from the trackers and by a detector of internally reflected Cherenkov light (DIRC), which measures the angle of the Cherenkov radiation cone. An electromagnetic calorimeter (EMC) consisting of an array of CsI(Tl) crystals measures the energy of photons and electrons.

We use a Monte Carlo (MC) simulation based on EvtGen [18] to optimize the event selection criteria. We model the background as $e^+e^- \to q\bar{q}$, $e^+e^- \to \tau^+\tau^-$ and $B\bar{B}$. We generate signal $B \to X_s\gamma$ with a uniform photon spectrum and then weight signal MC events so that the photon spectrum matches the kinematic-scheme model [19] with parameter values consistent with the previous *BABAR* $B \to X_s\gamma$ photon spectrum analysis ($m_b = 4.65$ GeV$/c^2$ and $\mu_\pi^2 = 0.20$ GeV^2) [20]. We use JETSET [21] as the fragmentation model and GEANT4 [22] to simulate the detector response.

IV. *B* RECONSTRUCTION

We reconstructed B meson candidates from 38 final states listed in Table I. The 16 modes marked with an asterisk (*) in Table I are used in the *CP* measurement. The other final states are either not flavor-specific final states or are low in yield. We reconstruct the unused modes in order to veto them after selecting the best candidate. In total, we use ten charged B final states and 6 neutral B final states in the A_{CP} measurement. These final states are the same as those used in a previous *BABAR* analysis [5].

Charged kaons and pions are selected from tracks classified with an error-correcting output code algorithm [17,23]. The classification uses SVT, DIRC, DCH, and EMC information. The kaon particle identification (PID) algorithm has approximately 90% efficiency and a pion-as-kaon misidentification rate of about 1%. Pion identification is roughly 99% efficient with a 15% kaon-as-pion misidentification rate.

Neutral kaons are reconstructed from the decay $K_S^0 \to \pi^+\pi^-$. The invariant mass of the two oppositely charged tracks is required to be between 489 and 507 MeV. The flight distance of the K_S^0 must be greater than 0.2 cm from the interaction point. The flight significance (defined as the flight distance divided by the uncertainty in the flight distance) of the K_S^0 must be greater than three. K_L^0 and $K_S^0 \to \pi^0\pi^0$ decays are not reconstructed for this analysis.

The neutral π^0 and η mesons are reconstructed from two photons. We require each photon to have energy of at least 30 MeV for π^0 and at least 50 MeV for η. The invariant mass of the two photons must be in the range of [115,150] MeV for π^0 candidates and in the range of [470,620] MeV for η candidates. Only π^0 and η candidates with momentum greater than 200 MeV$/c$ are used. We do not reconstruct $\eta \to \pi^+\pi^-\pi^0$ decays explicitly, but some are included in final states that contain $\pi^+\pi^-\pi^0$.

TABLE I. The 38 final states we reconstruct in this analysis. Charge conjugation is implied. The 16 final states used in the *CP* measurement are marked with an asterisk.

Number	Final state	Number	Final state
1*	$B^+ \to K_S\pi^+\gamma$	20	$B^0 \to K_S\pi^+\pi^-\pi^+\pi^-\gamma$
2*	$B^+ \to K^+\pi^0\gamma$	21	$B^0 \to K^+\pi^+\pi^-\pi^-\pi^0\gamma$
3*	$B^0 \to K^+\pi^-\gamma$	22	$B^0 \to K_S\pi^+\pi^-\pi^0\pi^0\gamma$
4	$B^0 \to K_S\pi^0\gamma$	23*	$B^+ \to K^+\eta\gamma$
5*	$B^+ \to K^+\pi^+\pi^-\gamma$	24	$B^0 \to K_S\eta\gamma$
6*	$B^+ \to K_S\pi^+\pi^0\gamma$	25	$B^+ \to K_S\eta\pi^+\gamma$
7*	$B^+ \to K^+\pi^0\pi^0\gamma$	26	$B^+ \to K^+\eta\pi^0\gamma$
8	$B^0 \to K_S\pi^+\pi^-\gamma$	27*	$B^0 \to K^+\eta\pi^-\gamma$
9*	$B^0 \to K^+\pi^-\pi^0\gamma$	28	$B^0 \to K_S\eta\pi^0\gamma$
10	$B^0 \to K_S\pi^0\pi^0\gamma$	29	$B^+ \to K^+\eta\pi^+\pi^-\gamma$
11*	$B^+ \to K_S\pi^+\pi^-\pi^+\gamma$	30	$B^+ \to K_S\eta\pi^+\pi^0\gamma$
12*	$B^+ \to K^+\pi^+\pi^-\pi^0\gamma$	31	$B^0 \to K_S\eta\pi^+\pi^-\gamma$
13*	$B^+ \to K_S\pi^+\pi^0\pi^0\gamma$	32	$B^0 \to K^+\eta\pi^-\pi^0\gamma$
14*	$B^0 \to K^+\pi^+\pi^-\pi^-\gamma$	33*	$B^+ \to K^+K^-K^+\gamma$
15	$B^0 \to K_S\pi^0\pi^+\pi^-\gamma$	34	$B^0 \to K^+K^-K_S\gamma$
16*	$B^0 \to K^+\pi^-\pi^0\pi^0\gamma$	35	$B^+ \to K^+K^-K_S\pi^+\gamma$
17	$B^+ \to K^+\pi^+\pi^-\pi^+\pi^-\gamma$	36	$B^+ \to K^+K^-K^+\pi^0\gamma$
18	$B^+ \to K_S\pi^+\pi^-\pi^+\pi^0\gamma$	37*	$B^0 \to K^+K^-K^+\pi^-\gamma$
19	$B^+ \to K^+\pi^+\pi^-\pi^0\pi^0\gamma$	38	$B^0 \to K^+K^-K_S\pi^0\gamma$

Each event is required to have at least one photon with energy $1.6 < E_\gamma^* < 3.0$ GeV, where the asterisk denotes variables measured in the $\Upsilon(4S)$ center-of-mass (CM) frame. These photons are used as the primary photon in reconstructing B mesons. Such a photon must have a lateral moment [2] less than 0.8 and the nearest EMC cluster must be at least 15 cm away. The angle of the photon momentum with respect to the beam axis must satisfy $-0.74 < \cos\theta < 0.93$.

We make some further preliminary requirements to reduce the data before giving events to the multivariate classifiers for final selection. The invariant mass of X_s (all daughters of the B candidate excluding the primary photon) must satisfy $0.6 < m_{X_s} < 3.2$ GeV$/c^2$. The X_s candidate is then combined with the primary photon to form a B candidate, which is required to have an energy-substituted mass $m_{\rm ES} = \sqrt{s/4 - p_B^{*2}}$, where p_B^* is the momentum of B in the CM frame, greater than 5.24 GeV$/c^2$. We also require the difference between half of the beam total energy and the energy of the reconstructed B in the CM frame, $|\Delta E| = |E^*_{\rm beam}/2 - E^*_B|$, to be less than 0.15 GeV. The angle between the thrust axis of the rest of the event(ROE) and the primary photon must satisfy $|\cos\theta^*_{T\gamma}| < 0.85$.

[2]The lateral moment is the ratio for the sum of energies of all but the two most energetic crystals in the cluster weighted by the squares of distances to the cluster center and the sum of energies of all crystals weighted by the square of distance to the cluster center.

V. EVENT AND CANDIDATE SELECTION

There are three main sources of background. The dominant source is continuum background, $e^+e^- \to q\bar{q}$. These events are more jet-like than the $e^+e^- \to \Upsilon(4S) \to B\bar{B}$. Thus, event shape variables provide discrimination. The continuum $m_{\rm ES}$ distribution does not peak at the B meson mass. The second background source is $B\bar{B}$ decays to final states other than $X_s\gamma$; hereafter we refer to these as generic $B\bar{B}$ decays. The third source is a cross-feed background which comes from actual $B \to X_s\gamma$ decays in which we fail to reconstruct the B in the correct final state. The $e^+e^- \to \tau^+\tau^-$ contribution is negligibly small.

We first place a preliminary selection on the ratio of angular moments[3] [24], $L_{12}/L_{10} < 0.46$ to reduce the number of the continuum background events. This ratio measures the jettiness of the event. Since the mass of the B meson is close to half the mass of the $\Upsilon(4S)$, the kinetic energy that the B meson can have is less than that available to $e^+e^- \to$ light quark pairs. Therefore, the signal peaks at a lower value of L_{12}/L_{10} than does the continuum background.

The B meson reconstruction typically yields multiple B candidates per event (∼10 on the average). To select the best candidate, we train a random forest classifier [25] based on $\Delta E/\sigma_E$, where σ_E is the uncertainty on the B candidate energy, the thrust of the reconstructed B candidate,[4] π^0 momentum, the invariant mass of the X_s system, and the zeroth and fifth Fox-Wolfram moments [26]. This signal selecting classifier (SSC) is trained on a large MC event sample to separate correctly reconstructed $B \to X_s\gamma$ decays from misreconstructed ones. For each event, the candidate with the maximum classifier output is chosen as the best candidate. This is the main difference from a previous *BABAR* analysis [5] which chose the event with the smallest $|\Delta E|$ as the best candidate. This method increases the efficiency by a factor of approximately two for the same misidentification rate. For example, selecting events with $m_{\rm ES} > 5.27$ GeV$/c^2$, at a fake rate of 25%, the signal rate is 16% for the $|\Delta E|$ selection and 33% for the SSC.

It should be emphasized that the best candidate selection procedure also selects final states in which the bottomness of the B cannot be deduced from the final decay products (flavor-ambiguous final states). After selecting the best candidate, we keep only events in which the best candidate is reconstructed with the final states marked with an asterisk in Table I. This removes events which are flavor-ambiguous final states from the A_{CP} measurement. Furthermore, because of the way the SSC was trained to discriminate against misreconstructed B candidates, SSC also provides good discriminating power against the generic $B\bar{B}$ background.

To further reduce the continuum background we build another random forest classifier, the background rejecting classifier (BRC), using the following variables:

(i) π^0 score: the output from a random forest classifier using the invariant mass of the primary photon with all other photons in the event and the energy of the other photons, which is trained to reject high-energy photons that come from the $\pi^0 \to \gamma\gamma$ decays.
(ii) Momentum flow[5] in 10° increments about the reconstructed B direction.
(iii) Zeroth-, first- and second-order angular moments along the primary photon axis computed in the CM frame of the ROE.
(iv) The ratio of the second and the zeroth angular moments described above.
(v) $|\cos\theta_B^*|$: the cosine of the angle between the B flight direction and the beam axis in the CM frame.
(vi) $|\cos\theta_T^*|$: the cosine of the angle between the thrust axis of the B candidate and the thrust axis of the ROE in the CM frame.
(vii) $|\cos\theta_{T\gamma}^*|$: the cosine of the angle between the primary photon momentum and the thrust axis of the ROE in the CM frame.

To obtain the best sensitivity, we simultaneously optimize, using MC samples, the SSC and BRC selections in four X_s mass ranges ([0.6–1.1], [1.1–2.0], [2.0–2.4], and [2.4–2.8]GeV$/c^2$), maximizing $S/\sqrt{S+B}$, where S is the number of expected signal events and B is the number of expected background events with $m_{\rm ES} > 5.27$ GeV$/c^2$. The optimized selection values are the same for both B and $\bar{B}$.

VI. FITTED ASYMMETRY

For each B flavor, we describe the $m_{\rm ES}$ distribution with a sum of an ARGUS distribution [27][6] and a two-piece normal distribution (G)[7]:

[3]The Legendre moment of momentum for a given axis.

[4]
$$\text{Thrust} = \max_A \left[\frac{\sum_{i=1}^N |A \cdot p_i|}{\sum_{i=1}^N \sqrt{p_i \cdot p_i}}\right]$$
where A is a unit vector and p_i are three momenta of the decay particles of the B candidate.

[5]The scalar sum of all momenta within a cone of a given opening angle about a given axis.

[6]
$$\text{ARGUS}(x;c,\chi,p) = \frac{2^{-p}\chi^{2(p+1)}}{\Gamma(p+1)-\Gamma(p+1,\frac{1}{2}\chi^2)} \times \frac{x}{c^2}\left(1-\frac{x^2}{c^2}\right)^p \exp\left\{-\frac{1}{2}\chi^2\left(1-\frac{x^2}{c^2}\right)\right\}$$

[7]
$$\text{G}(x;\mu,\sigma_L,\sigma_R) = N \times \begin{cases} \exp\left\{\frac{(x-\mu)^2}{2\sigma_L^2}\right\} & \text{if } x < \mu \\ \exp\left\{\frac{(x-\mu)^2}{2\sigma_R^2}\right\} & \text{if } x \geq \mu \end{cases},$$
where N is the normalization.

$$\mathrm{PDF}^{b}(m_{\mathrm{ES}}) = \frac{T_{\mathrm{cont}}}{2}(1+A_{\mathrm{cont}})\mathrm{ARGUS}(m_{\mathrm{ES}};c^{b},\chi^{b},p^{b}) + \frac{T_{\mathrm{peak}}}{2}(1+A_{\mathrm{peak}})G(m_{\mathrm{ES}};\mu^{b},\sigma_{L}^{b},\sigma_{R}^{b}), \quad (4)$$

$$\mathrm{PDF}^{\bar{b}}(m_{\mathrm{ES}}) = \frac{T_{\mathrm{cont}}}{2}(1-A_{\mathrm{cont}})\mathrm{ARGUS}(m_{\mathrm{ES}};c^{\bar{b}},\chi^{\bar{b}},p^{\bar{b}}) + \frac{T_{\mathrm{peak}}}{2}(1-A_{\mathrm{peak}})G(m_{\mathrm{ES}};\mu^{\bar{b}},\sigma_{L}^{\bar{b}},\sigma_{R}^{\bar{b}}) \quad (5)$$

where

$$T_{\mathrm{cont}} = n_{\mathrm{cont}}^{b} + n_{\mathrm{cont}}^{\bar{b}}, \quad (6)$$

$$T_{\mathrm{peak}} = n_{\mathrm{peak}}^{b} + n_{\mathrm{peak}}^{\bar{b}} \quad (7)$$

are the total number of events of both flavors described by the ARGUS distribution and the two-piece normal distribution and

$$A_{\mathrm{cont}} = \frac{n_{\mathrm{cont}}^{b} - n_{\mathrm{cont}}^{\bar{b}}}{n_{\mathrm{cont}}^{b} + n_{\mathrm{cont}}^{\bar{b}}}, \quad (8)$$

$$A_{\mathrm{peak}} = \frac{n_{\mathrm{peak}}^{b} - n_{\mathrm{peak}}^{\bar{b}}}{n_{\mathrm{peak}}^{b} + n_{\mathrm{peak}}^{\bar{b}}} \quad (9)$$

are the flavor asymmetries of events described by the ARGUS distribution and the two-piece normal distribution, respectively. The superscript b and $\bar{b}$ indicate whether the parameter belongs to the b quark containing B meson

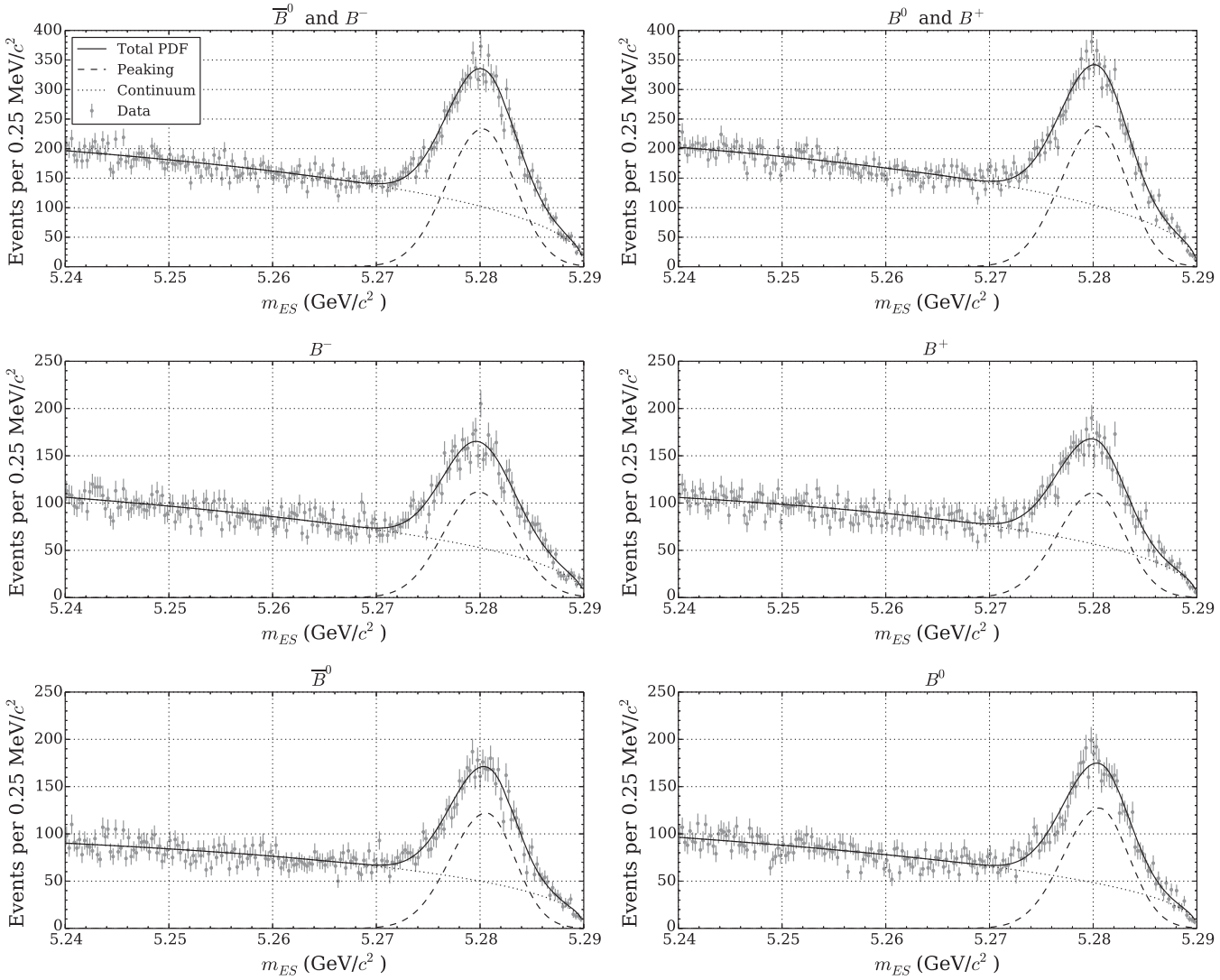

FIG. 1. The m_{ES} distributions along with fitted probability density functions, for: $\bar{B}^0$ and B^- sample (top left), B^0 and B^+ sample (top right), B^- sample (middle left), B^+ sample (middle right), $\bar{B}^0$ sample (bottom left), and B^0 sample (bottom right). Data are shown as points with error bars. The ARGUS distribution component, two-piece normal distribution component and the total probability density function are shown with dotted lines, dashed lines, and solid lines, respectively.

TABLE II. Summary of A_{CP} results along with $A_{\rm det}$ and systematic uncertainties due to peaking background contamination (D) for each B sample. The A_{CP}'s in the last column are calculated using Eq. (3). The first error is statistical, the second (if present) is systematics.

B Sample	$A_{\rm peak}$	D	$A_{\rm det}$	A_{CP}
All B	$+(0.33 \pm 1.87)\%$	$\pm 0.88\%$	$-(1.40 \pm 0.49 \pm 0.51)\%$	$+(1.73 \pm 1.93 \pm 1.02)\%$
Charged B	$+(3.14 \pm 2.86)\%$	$\pm 0.80\%$	$-(1.09 \pm 0.67 \pm 0.51)\%$	$+(4.23 \pm 2.93 \pm 0.95)\%$
Neutral B	$-(2.48 \pm 2.47)\%$	$\pm 0.97\%$	$-(1.74 \pm 0.72 \pm 0.51)\%$	$-(0.74 \pm 2.57 \pm 1.10)\%$

($\bar{B}^0$ and B^-) distribution or the $\bar{b}$ quark containing B meson distribution (B^0 and B^+), respectively. In particular, $n^b_{\rm peak}$ and $n^{\bar{b}}_{\rm peak}$ are the numbers of events in the peaking (Gaussian) part of the distribution. Similarly, $n^b_{\rm cont}$ and $n^{\bar{b}}_{\rm cont}$ are the numbers of events in the continuum (ARGUS) part of the distribution. The shape parameters for ARGUS distributions are the curvatures (χ^b and $\chi^{\bar{b}}$), the powers (p^b and $p^{\bar{b}}$), and the endpoint energies (c^b and $c^{\bar{b}}$). The shape parameters for two-piece normal distribution are the peak locations (μ^b and $\mu^{\bar{b}}$), the left-side widths (σ^b_L and $\sigma^{\bar{b}}_L$), and the right-side widths (σ^b_R and $\sigma^{\bar{b}}_R$).

It should be noted that $A_{\rm peak}$ is related to A_{CP} defined in Eq. (1) by the relation shown in Eq. (3). To obtain $A_{\rm peak}$, we perform a simultaneous binned likelihood fit for both B flavors. The ARGUS endpoint energies c^b and $c^{\bar{b}}$ are fixed at $5.29\ {\rm GeV}/c^2$. All other shape parameters for the ARGUS distributions and the two-piece normal distributions are allowed to float separately. Fig. 1 shows the $m_{\rm ES}$ distributions, along with fitted shapes. Table II summarizes the results for $A_{\rm peak}$.

VII. DETECTOR ASYMMETRY

Part of the difference between $A_{\rm peak}$ and A_{CP} comes from the difference in K^+ and K^- efficiencies. The K^+ PID efficiency is slightly higher than the K^- PID efficiency; the difference also varies with the track momentum. The cause of this difference is the fact that the cross section for K^--hadron interactions is higher than that for K^+-hadron interactions. This translates to the K^- having a greater probability of interacting before it reaches the DIRC, thereby lowering the quality of the K^- Cherenkov cone angle measurement, which affects the PID performance.

The first order correction to A_{CP} from K^+/K^- efficiency differences is given by

$$A_{\rm det} = \frac{\nu_b - \nu_{\bar{b}}}{\nu_b + \nu_{\bar{b}}}, \tag{10}$$

where ν_b and $\nu_{\bar{b}}$ are the number of events for each flavor after all selections, assuming the underlying physics has no flavor asymmetry.

We use a sideband region ($m_{\rm ES} < 5.27\ {\rm GeV}/c^2$) which consists mostly of $e^+e^- \to q\bar{q}$ events to measure $A_{\rm det}$. We do not expect a flavor asymmetry in the underlying physics in this region. We count the number of events in the sideband region for each flavor and use Eq. (10) to determine $A^{\rm sideband}_{\rm det}$.

However, since the difference in K^- and K^+ hadron cross section depends on K momentum and the K momentum distributions of the side band region and the peaking region ($m_{\rm ES} > 5.27\ {\rm GeV}/c^2$) slightly differ, $A^{\rm sideband}_{\rm det}$ and $A_{\rm det}$ need not be identical. The variation of $A_{\rm det}$ for any K momentum distribution can be bounded by the maximum and minimum value of the ratio between K^+ and K^- efficiencies ($\epsilon_{K^+}/\epsilon_{K^-}$) in the K momentum range of interest:

$$\frac{1}{2}\left(\min_{p_K}\frac{\epsilon_{K^+}}{\epsilon_{K^-}} - 1\right) \le A_{\rm det} \le \frac{1}{2}\left(\max_{p_K}\frac{\epsilon_{K^+}}{\epsilon_{K^-}} - 1\right). \tag{11}$$

The final states with no charged K can be considered as having a special value of p_K where ϵ_{K^+} and ϵ_{K^-} are identical.

We use highly pure samples of charged kaons from the decay $D^{*+} \to D^0\pi^+$, followed by $D^0 \to K^-\pi^+$, and its charge conjugate, to measure the ratio of efficiencies for K^+ and K^-. We find that the deviation from unity of $\epsilon_{K^+}/\epsilon_{K^-}$ varies from 0% to 2.5% depending on the track momentum.

The bound given in Eq. (11) implies that the distribution of the differences between any two detector asymmetries chosen uniformly within the bound is a triangle distribution with the base width of 2.5%.

The standard deviation of such a distribution is $2.5\%/\sqrt{24} = 0.5\%$. We use $A^{\rm sideband}_{\rm det}$ as the central value for $A_{\rm det}$ and this standard deviation as the systematic uncertainty associated with detector asymmetry. Table II lists the results of $A_{\rm det}$.

VIII. PEAKING BACKGROUND CONTAMINATION

Our fitting procedure does not explicitly separate the generic $B\bar{B}$ backgrounds and cross feed from the signal. Both backgrounds have small peaking components, as shown in Fig. 2, so the yield for each flavor used in calculating $A_{\rm peak}$ contains both signal and these peaking backgrounds. We quantify the effect and include it as a source of systematic uncertainty.

Let the number of signal events for b quark containing B mesons and $\bar{b}$ quark containing B mesons be n_b and $n_{\bar{b}}$ and

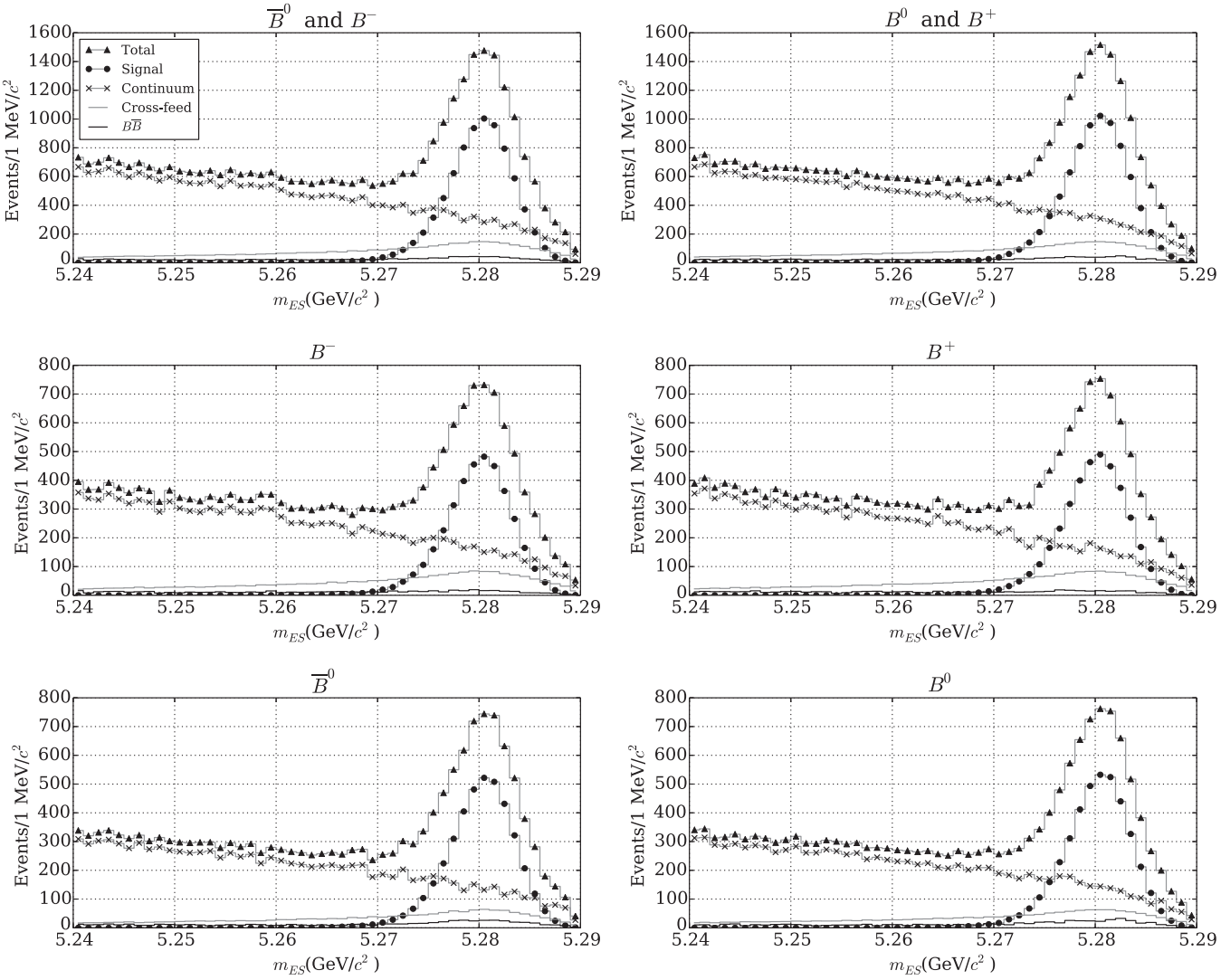

FIG. 2. The contributions to the total $m_{\rm ES}$ distributions (gray lines with triangle markers) from the signal $B \to X_s\gamma$ (gray lines with circle markers), the continuum background (gray lines with x markers), the cross-feed background (gray lines with no marker), and the generic $B\bar{B}$ background (solid black lines) according to the MC sample for: $\bar{B}^0$ and B^- sample (top left), B^0 and B^+ sample (top right), B^- sample (middle left), B^+ sample (middle right), $\bar{B}^0$ sample (bottom left), and B^0 sample (bottom right).

the number of contaminating peaking background events misreconstructed as b quark containing B mesons and $\bar{b}$ quark containing B mesons be β_b and $\beta_{\bar{b}}$. The difference between $A_{\rm peak}$ and A_{CP} due to peaking background contamination is given by

$$D = R \times \delta A, \tag{12}$$

where R is the ratio of the number of peaking background events to the total number of events in the peaking region, given by

$$R = \frac{\beta_b + \beta_{\bar{b}}}{n_b + n_{\bar{b}} + \beta_b + \beta_{\bar{b}}}, \tag{13}$$

and δA is the difference between the true signal asymmetry and the peaking background asymmetry, given by

$$\delta A = \frac{n_b - n_{\bar{b}}}{n_b + n_{\bar{b}}} - \frac{\beta_b - \beta_{\bar{b}}}{\beta_b + \beta_{\bar{b}}}. \tag{14}$$

We estimate R using the MC sample. We use the sum of the expected number of cross-feed background events and expected number of generic $B\bar{B}$ events with $m_{\rm ES} > 5.27$ GeV$/c^2$ for each flavor as β_b and $\beta_{\bar{b}}$. We obtain n_b and $n_{\bar{b}}$ from the total number of expected signal events for each flavor.

Since the peaking background events are from misreconstructed B mesons, the $m_{\rm ES}$ distribution of the peaking background has a very long tail. It resembles the sum of an ARGUS distribution and a small peaking part. The fit to the total $m_{\rm ES}$ distribution is the sum of a two-piece normal distribution and an ARGUS distribution. A significant portion of peaking background is absorbed into the

TABLE III. Values of R, δA and D.

B Sample	R	$\lvert\delta A\rvert$	D
All B	0.26	3.4%	±0.88%
Charged B	0.28	3.4%	±0.80%
Neutral B	0.24	3.4%	±0.97%

ARGUS distribution causing our estimate of R to be overestimated.

We bound the difference in asymmetry, δA, using the range of values predicted by the SM: $-0.6\% < A_{CP}^{\rm SM} < 2.8\%$. This gives $|\delta A| < 3.4\%$. This value is also very conservative, since the amount of cross-feed background in the signal region is approximately five times the amount of generic $B\bar{B}$ background, and we expect the flavor asymmetry of the cross-feed events to be similar to that of the signal. The asymmetry from the generic $B\bar{B}$ background is expected to be small.

To provide a check of our estimate of the cross-feed contribution to $A_{\rm peak}$, we extract $A_{\rm peak}$ from pseudo MC experiments with varying amounts of cross-feed background asymmetry and observe the shift from the true value of the signal asymmetry. A shift due to cross feed is expected in this study, since we allow the cross-feed asymmetry to be different than for the signal. The shift is about half the value estimated using the method described above. The difference is expected because the cross feed (and generic $B\bar{B}$) has a very long tail, so that only part of it will be included in the peaking component, the remainder gets absorbed in the ARGUS component, as we have noted above. Thus, we obtain a result that is expected, but in the end we use a more conservative estimate for the systematic uncertainty in the asymmetry from peaking background. We do this because we wish to avoid relying on the MC model for the peaking part of the cross feed. For A_{CP} of the charged and neutral B, this estimate is conservative enough to cover a large possible range of $|\Delta A_{X_s\gamma}| < 15\%$ that could shift the value of $A_{\rm peak}$ via the cross feed of the type $\bar{B}^0 \to X_s\gamma$ misreconstructed as $B^- \to X_s\gamma$ ($\bar{B}^0 \Rightarrow B^-$) and $B^- \to X_s\gamma$ misreconstructed as $\bar{B}^0 \to X_s\gamma$ ($B^- \Rightarrow \bar{B}^0$). Table III lists the values of R, δA and D.

IX. RESULTS

Following Eq. (3), we subtract $A_{\rm det}$ from $A_{\rm peak}$ to obtain A_{CP}. The statistical uncertainties are added in quadrature. Systematic uncertainties from peaking background contamination and from detector asymmetry are added in quadrature to obtain the total systematic uncertainty. We find

$$A_{CP} = +(1.7 \pm 1.9 \pm 1.0)\%, \tag{15}$$

where the uncertainties are statistical and systematic, respectively. Compared to the current world average, the statistical uncertainty is smaller by approximately 1/3 due to the improved rejection of peaking background described above.

The measurement of A_{CP} is based on the ratio of the number of events, but A_{CP} is defined as the ratio of widths. In order to make the two definitions of A_{CP} equivalent, we make two assumptions. First, we assume that there are as many decaying B^0 mesons as decaying $\bar{B}^0$ mesons, i.e. there is no CP violation in mixing. This has been measured to be at most a few 10^{-3} for B mesons [8]. Second, since the ratio of the number of events is essentially the ratio of the branching fractions under the first assumption, we assume that the lifetime of b - and $\bar{b}$ -containing B mesons are identical so that the ratio of the branching fractions is equal to the ratio of the decay widths. This is guaranteed if we assume CPT invariance. The isospin asymmetry has negligible effect on A_{CP}: The effect from the difference of B^0 and B^+ lifetime and from $\Delta A_{X_s\gamma}$ is suppressed by a factor of isospin efficiency asymmetry,[8] which we find to be on the order of 2%. The total effect is thus on the order of 10^{-4}, which is below our sensitivity.

Using the values of A_{CP} for charged B and neutral B in Table II, we find

$$\Delta A_{X_s\gamma} = +(5.0 \pm 3.9 \pm 1.5)\%, \tag{16}$$

where the uncertainties are statistical and systematic, respectively. The statistical and systematic uncertainties on $\Delta A_{X_s\gamma}$ are obtained by summing in quadrature the uncertainties on the charged and neutral A_{CP} measurements.

The systematic uncertainty for $\Delta A_{X_s\gamma}$ is also validated with an alternative method of estimating the multiplicative effects from the peaking background contamination on $\Delta A_{X_s\gamma}$ taking into account each component of the cross feed. In particular, the cross feeds of the types $\bar{B}^0 \Rightarrow B^-$ and $B^- \Rightarrow \bar{B}^0$ produce shifts that are proportional to $\Delta A_{X_s\gamma}$. This is because such a cross feed adds a contribution from the other asymmetry, and hence introduces a shift that dilutes the measured $\Delta A_{X_s\gamma}$. If $\Delta A_{X_s\gamma} = 0$, then there is no shift from cross feed. A similar proportionality of the shift on $\Delta A_{X_s\gamma}$ occurs for generic $B\bar{B}$ background, assuming negligible asymmetry in this background, and in the limit of equal background fractions to B^0 and B^-. We use a conservative value for the peaking background composition of $2:2:1$ ($\bar{B}^0 \Rightarrow \bar{B}^0 : B^- \Rightarrow \bar{B}^0 :$ generic $B\bar{B}$) and the value of cross-feed contamination ratio $R \sim 1/4$. We also assume that the contributions from $\bar{B}^0 \Rightarrow B^-$ and $B^- \Rightarrow \bar{B}^0$ are equal. We find the total effect to be conservatively at most $\frac{1}{4}\Delta A_{X_s\gamma} = 1.3\%$. The estimate is in agreement with the quadrature sum of the peaking background contamination systematics for charged and neutral B asymmetry, which is $\sqrt{1.0\%^2 + 0.8\%^2} = 1.3\%$.

[8]The ratio of the difference between charged and neutral B efficiency to the sum of the two.

In the calculation of $\Delta A_{X_s\gamma}$, we also assume that the fragmentation does not create an additional asymmetry. This is generally assumed in this type of analysis. This is particularly important for the $\Delta A_{X_s\gamma}$ measurement since the final states are not all isospin counterparts. With this assumption, we can use A_{CP} for 10 charged B final states and A_{CP} for 6 neutral B final states as A_{CP} for charged B and neutral B, respectively.

Using the formula,

$$\Delta A_{X_s\gamma} \simeq 0.12 \times \frac{\tilde{\Lambda}_{78}}{100\ \text{MeV}} \text{Im}(C_{8g}/C_{7\gamma}), \qquad (17)$$

given in [9], we can use the measured value of $\Delta A_{X_s\gamma}$ to determine the 68% and 90% confidence limits (C.L.) on $\text{Im}(C_{8g}/C_{7\gamma})$. The interference amplitude, $\tilde{\Lambda}_{78}$, in Eq. (17) is only known as a range of possible values,

$$17\ \text{MeV} < \tilde{\Lambda}_{78} < 190\ \text{MeV}. \qquad (18)$$

We calculate a quantity called minimum χ^2 defined by

$$\text{minimum } \chi^2 = \frac{\min_{\tilde{\Lambda}_{78}}[(\Delta A_{\text{Th}} - \Delta A_{\text{Exp}})^2]}{\sigma^2}, \qquad (19)$$

where ΔA_{Th} is the theoretical prediction of $\Delta A_{X_s\gamma}$ for given $\text{Im}(C_{8g}/C_{7\gamma})$ and $\tilde{\Lambda}_{78}$ using Eq. (17), ΔA_{Exp} is the measured value, σ is uncertainty on the measured value, and the minimum is taken over the range of $\tilde{\Lambda}_{78}$ given in Eq. (18). Figure 3 shows the plot of minimum χ^2 versus $\text{Im}(C_{8g}/C_{7\gamma})$. It has two notable features. First, there is a plateau of minimum $\chi^2 = 0$. This is the region of $\text{Im}(C_{8g}/C_{7\gamma})$ where we can always find a value of $\tilde{\Lambda}_{78}$ within the possible range [Eq. (18)] such that ΔA_{Th} matches exactly ΔA_{Exp}. Second, the discontinuity at $\text{Im}(C_{8g}/C_{7\gamma}) = 0$ comes from the fact that the value of $\tilde{\Lambda}_{78}$ that gives the minimum value is different. When $\text{Im}(C_{8g}/C_{7\gamma})$ is small and positive, we need a large positive $\tilde{\Lambda}_{78}$ to be as close as possible to the measured value, while when $\text{Im}(C_{8g}/C_{7\gamma})$ is negative, we need a small positive value of $\tilde{\Lambda}_{78}$ to not be too far from the measured value.

The 68% and 90% confidence limits are then obtained from the ranges of $\text{Im}(C_{8g}/C_{7\gamma})$, which yield the minimum χ^2 less than 1 and 4, respectively. We find

$$0.07 \le \text{Im}\frac{C_{8g}}{C_{7\gamma}} \le 4.48, \qquad 68\%\ \text{C.L.}, \qquad (20)$$

$$-1.64 \le \text{Im}\frac{C_{8g}}{C_{7\gamma}} \le 6.52, \qquad 90\%\ \text{C.L.} \qquad (21)$$

The dependence of minimum χ^2 on $\text{Im}(C_{8g}/C_{7\gamma})$ as shown in Fig. 3 is not parabolic, which would be expected from a Gaussian probability. Care must be taken when combining it with other constraints. Since the confidence intervals obtained are dominated by the possible values $\tilde{\Lambda}_{78}$ at the low end, improvement of limits on $\tilde{\Lambda}_{78}$ will narrow the confidence interval. We therefore also provide a confidence interval for $\text{Im}(C_{8g}/C_{7\gamma})$ as the function of $\tilde{\Lambda}_{78}$ in Fig. 4.

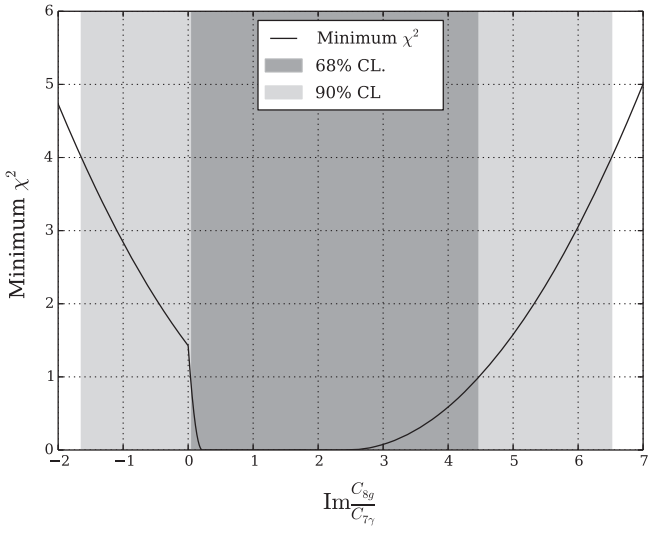

FIG. 3. The minimum χ^2 for given $\text{Im}\frac{C_{8g}}{C_{7\gamma}}$ from all possible values of $\tilde{\Lambda}_{78}$. 68% and 90% confidence intervals are shown in dark gray and light gray, respectively.

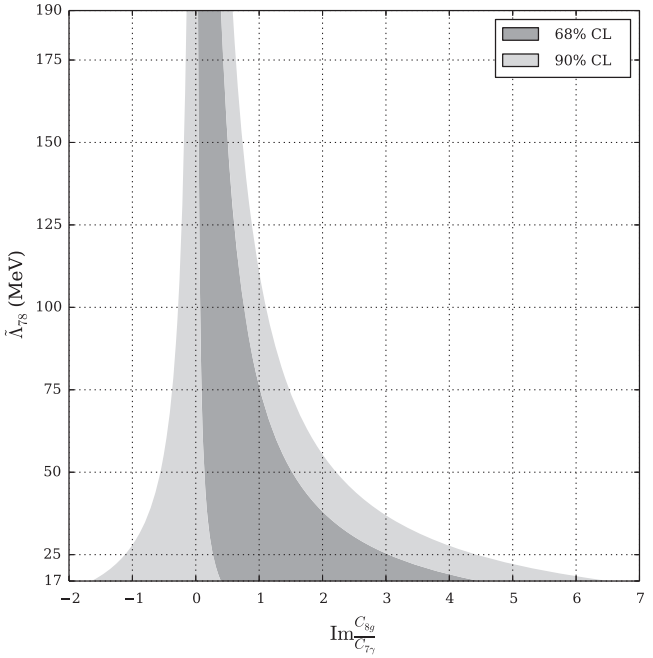

FIG. 4. The 68% and 90% confidence intervals for $\text{Im}\frac{C_{8g}}{C_{7\gamma}}$ and $\tilde{\Lambda}_{78}$.

X. SUMMARY

In conclusion, we present a measurement of the direct CP violation asymmetry, A_{CP}, in $B \to X_s\gamma$ and the isospin difference of the asymmetry, $\Delta A_{X_s\gamma}$ with 429 fb^{-1} of data collected at the $\Upsilon(4S)$ resonance with the *BABAR* detector. B meson candidates are reconstructed from 10 charged B final states and 6 neutral B final states. We find $A_{CP} = +(1.7 \pm 1.9 \pm 1.0)\%$, in agreement with the SM prediction and with the uncertainty smaller than that of the current world average. We also report the first measurement of $\Delta A_{X_s\gamma} = +(5.0 \pm 3.9 \pm 1.5)\%$, consistent with the SM prediction. Using the value of $\Delta A_{X_s\gamma}$, we calculate the 68% and 90% confidence intervals for $\mathrm{Im}(C_{8g}/C_{7\gamma})$ shown in Eqs. (20) and (21), respectively. The confidence interval can be combined with existing constraints on $C_{7\gamma}$ to provide a constraint on C_{8g}.

ACKNOWLEDGMENTS

We would like to thank Gil Paz for very useful discussions. We are grateful for the extraordinary contributions of our PEP-II colleagues in achieving the excellent luminosity and machine conditions that have made this work possible. The success of this project also relies critically on the expertise and dedication of the computing organizations that support *BABAR*. The collaborating institutions wish to thank SLAC for its support and the kind hospitality extended to them. This work is supported by the U.S. Department of Energy and National Science Foundation, the Natural Sciences and Engineering Research Council (Canada), the Commissariat à l'Energie Atomique and Institut National de Physique Nucléaire et de Physique des Particules (France), the Bundesministerium für Bildung und Forschung and Deutsche Forschungsgemeinschaft (Germany), the Istituto Nazionale di Fisica Nucleare (Italy), the Foundation for Fundamental Research on Matter (The Netherlands), the Research Council of Norway, the Ministry of Education and Science of the Russian Federation, Ministerio de Economía y Competitividad (Spain), the Science and Technology Facilities Council (United Kingdom), and the Binational Science Foundation (U.S.-Israel). Individuals have received support from the Marie-Curie IEF program (European Union) and the A. P. Sloan Foundation (USA).

[1] A. L. Kagan and M. Neubert, Phys. Rev. D **58**, 094012 (1998).
[2] T. Hurth, E. Lunghi, and W. Porod, Nucl. Phys. **B704**, 56 (2005).
[3] L. Wolfenstein and Y. L. Wu, Phys. Rev. Lett. **73**, 2809 (1994).
[4] C.-K. Chua, X.-G. He, and W.-S. Hou, Phys. Rev. D **60**, 014003 (1999).
[5] B. Aubert *et al.* (*BABAR* Collaboration), Phys. Rev. Lett. **101**, 171804 (2008).
[6] S. Nishida *et al.* (BELLE Collaboration), Phys. Rev. Lett. **93**, 031803 (2004).
[7] T. E. Coan *et al.* (CLEO Collaboration), Phys. Rev. Lett. **86**, 5661 (2001).
[8] J. Beringer *et al.* (Particle Data Group), Phys. Rev. D **86**, 010001 (2012).
[9] M. Benzke, S. J. Lee, M. Neubert, and G. Paz, Phys. Rev. Lett. **106**, 141801 (2011).
[10] M. Jung, X.-Q. Li, and A. Pich, J. High Energy Phys. 10 (2012) 063.
[11] A. Hayakawa, Y. Shimizu, M. Tanimoto, and K. Yamamoto, Phys. Lett. B **710**, 446 (2012).
[12] W. Altmannshofer, P. Paradisi, and D. M. Straub, J. High Energy Phys. 04 (2012) 008.
[13] J. P. Lees *et al.* (*BABAR* Collaboration), Phys. Rev. D **86**, 052012 (2012).
[14] J. P. Lees *et al.* (*BABAR* Collaboration), Phys. Rev. D **86**, 112008 (2012).
[15] J. P. Lees *et al.* (*BABAR* Collaboration), Nucl. Instrum. Methods Phys. Res., Sect. A **726**, 203 (2013).
[16] B. Aubert *et al.* (*BABAR* Collaboration), Nucl. Instrum. Methods Phys. Res., Sect. A **479**, 1 (2002).
[17] B. Aubert *et al.* (*BABAR* Collaboration) Nucl. Instrum. Methods Phys. Res., Sect. A **729**, 615 (2013).
[18] D. J. Lange, Nucl. Instrum. Methods Phys. Res., Sect. A **462**, 152 (2001).
[19] D. Benson, I. I. Bigi, and N. Uraltsev, Nucl. Phys. **B710**, 371 (2005).
[20] B. Aubert *et al.* (*BABAR* Collaboration), Phys. Rev. D **72**, 052004 (2005).
[21] T. Sjostrand, Comput. Phys. Commun. **82**, 74 (1994).
[22] S. Agostinelli *et al.*, Nucl. Instrum. Methods Phys. Res., Sect. A **506**, 250 (2003).
[23] T. G. Dietterich and G. Bakiri, J. Artif. Intell. Res. **2**, 263 (1995).
[24] B. Aubert *et al.* (*BABAR* Collaboration), Phys. Rev. Lett. **89**, 281802 (2002).
[25] L. Breiman, Mach. Learn. **45**, 5 (2001).
[26] G. Fox and S. Wolfram, Phys. Rev. Lett. **41**, 1581 (1978).
[27] H. Albrecht *et al.* (ARGUS Collaboration), Phys. Lett. B **241**, 278 (1990).